Soft Matter

PAPER

View Article Online
View Journal | View Issue

Cite this: *Soft Matter*, 2021, 17, 6627

Liquid–liquid crystalline phase separation in biological filamentous colloids: nucleation, growth and order–order transitions of cholesteric tactoids†

Paride Azzari, [a] Massimo Bagnani [a] and Raffaele Mezzenga *[ab]

The process of liquid–liquid crystalline phase separation (LLCPS) in filamentous colloids is at the very core of multiple biological, physical and technological processes of broad significance. However, the complete theoretical understanding of the process is still missing. LLCPS involves the nucleation, growth and up-concentration of anisotropic droplets from a continuous isotropic phase, until a state of equilibrium is reached. Herein, by combining the thermodynamic extremum principle with the Onsager theory, we describe the nucleation and growth of liquid crystalline droplets, and the evolution of their size and concentration during phase separation, eventually leading to a multitude of order–order phase transitions. Furthermore, a decreasing pitch behaviour can be predicted using this combined theory during tactoid growth, already observed experimentally but not yet explained by present theories. The results of this study are compared with the experimental data of cholesteric pitch, observed in three different systems of biological chiral liquid crystals. These findings give an important framework for predicting the formation, growth and phase behaviour of biological filamentous colloids undergoing LLCPS, advancing our understanding of liquid–liquid phase separation and self-assembly mechanisms in biological systems, and provide a valuable rationale for developing nanomaterials and applications in nanotechnology.

Received 27th March 2021,
Accepted 28th May 2021

DOI: 10.1039/d1sm00466b

rsc.li/soft-matter-journal

1 Introduction

Phase separation is a fundamental phenomenon observed in various branches of materials science, from superconductors to soft matter.[1] Polymeric fluids or colloidal dispersions are just an example of systems undergoing a phase separation,[2] where a single phase in a supersaturated state evolves into two different thermodynamically stable phases.[3] These liquid states display distinct physical properties and different structures, even though their components are chemically identical.[4] This phenomenon is called liquid–liquid phase separation (LLPS),[5] which can be achieved by changing the pressure, temperature or concentration.[6] Liquid–liquid phase separation in biology is associated with a multitude of cellular functions and structures,[7] such as in membrane-less organelles,[8] and understanding this process has important implications in the elucidation of several mechanisms of life functioning. The most common form of liquid–liquid phase separation involves two biopolymers (*e.g.* a protein and RNA)[9] and is primarily regulated by enthalpic interactions.[7] The classical system is therefore a two-component system in nature (in addition to the background solvent). In stark contrast, phase separation involving only one hydrocolloid component can occur on a purely entropic basis when the colloid is of filamentous type and has a large associated excluded volume. We refer to this type of 1-component (plus solvent) liquid–liquid phase separation as liquid–liquid crystalline phase separation (LLCPS) to fundamentally distinguish it from the LLPS introduced above. The thermodynamic description of the underlying physics is deeply rooted into the seminal formalism proposed by Onsager.[10] More precisely, when the two liquids are distinguished by a different orientational distribution of the constituents, as in the case of liquid crystals,[11] the two phases are called nematic and isotropic, for the ordered and unordered phase, respectively. In this case, the onset of phase separation is characterized by the formation of microdroplets of the nematic phase, from a supersaturated isotropic bulk phase.[12] These nematic droplets are known as tactoids, and during phase separation, their shape and nematic director field configuration can change spontaneously, with increasing

[a] *Department of Health Sciences and Technology, ETH Zürich, 8092 Zürich, Switzerland. E-mail: raffaele.mezzenga@hest.ethz.ch*
[b] *Department of Materials, ETH Zürich, 8093 Zürich, Switzerland*

† Electronic supplementary information (ESI) available. See DOI: 10.1039/d1sm00466b

volumes.[13–15] This becomes particularly significant when the filamentous colloid building blocks are chiral, with macroscopic chirality of the droplets also emerging during growth and leading to the formation of chiral nematic (or cholesteric) tactoidal droplets.[16–18] The shape of these classes of tactoids has already been rationalized by the interaction between confinement, anisotropic surface energy, and Frank–Oseen elastic energy.[19,20] To date, however, several thermodynamic, structural and kinetic aspects of this LLCPS process remain still unclear, such as the nature of the transitions between the different configurations, the dynamics of the growth process, and the change in cholesteric periodicity (pitch) observed with increasing volumes of the droplets. This latter effect has been observed experimentally in different chiral systems,[18,21] and requires a more refined analysis to be explained, since the confinement effects are not sufficient to elucidate this phenomenon.

Here, we propose a theoretical description of the nucleation and growth phases of the tactoids during the LLCPS process, following the evolution of the composition of binodal lines describing the phase transition. In particular, we show that such phase separation leads to a change in the concentration, eventually leading to a change in the pitch of the cholesteric phase, *i.e.* during their growth, therefore having a pitch that decreases with an increase in the volume. To support these theoretical findings, we benchmark the theory with experimental data and successfully describe the evolution of pitch in cholesteric tactoids, obtained from three different systems of biological colloids: β-lactoglobulin (BLG) amyloid fibrils,[20] carboxylated cellulose nanocrystals (C-CNCs)[18] and sulfurated cellulose nanocrystals (S-CNCs).[22]

2 Phase behaviour: Onsager theory

There are various theories describing the phase behaviour in liquid crystals from Flory[23] and Straley.[24] A review of different approaches can be seen in ref. 25 The Onsager theory[10] predicts accurately the phase boundaries of nematic and isotropic phases for the three systems under analysis, even though they are composed of charged polydisperse rods.[21,26] The rods considered have a contour length well below the persistence length and deflection length, and therefore they can be considered effectively rigid rods.[26] Moreover, the theory allows computing pressure and chemical potential at each concentration.

As a base for the discussion we briefly recapitulate the Onsager theory following his groundbreaking work.[10] We define the excess free energy F of a volume V, containing N hard rods of diameter D and length L as

$$F = Nk_{\mathrm{B}}T\left(\log\frac{N}{V} - 1 + \sigma_1(f) + b\frac{N}{V}\sigma_2(f)\right), \qquad (1)$$

where $b = \frac{\pi}{4}L^2D$ is half the excluded volume between two randomly oriented rods and σ_1 and σ_2 are functions of the distribution function f of the angle Θ between the rods and the director field; for a detailed description see ref. 27. The derivatives of F with respect to V and N are called respectively osmotic pressure (Π) and chemical potential (μ):

$$\Pi = -\frac{\partial F}{\partial V} = k_{\mathrm{B}}T\left(\frac{N}{V} + b\frac{N^2}{V^2}\sigma_2(f)\right); \qquad (2)$$

$$\mu = \frac{\partial F}{\partial N} = k_{\mathrm{B}}T\left(\log\frac{N}{V} + \sigma_1(f) + 2b\frac{N}{V}\sigma_2(f)\right). \qquad (3)$$

The isotropic distribution, where all directions are equally probable, $f_i = \frac{1}{4\pi}$, results in $\sigma_1(f_i) = 0$ and $\sigma_2(f_i) = 1$, see ESI† for details. In the case of an anisotropic distribution, where f is not a constant, Onsager's trial function $f_\alpha(\Theta) = \frac{\alpha}{4\pi}\sinh\alpha\cosh(\alpha\cos\Theta)$ can be used. In case of large α, $\sigma_1(f_\alpha)$ and $\sigma_2(f_\alpha)$ can be substituted by their asymptotic series (ESI†). This parametrization allows F to be minimized at each rescaled concentration $\phi = b\frac{N}{V} = \frac{L}{D}\varphi$, where φ is the volume fraction of the rods. Fig. 1(a) (purple line) shows the order parameter S for increasing concentration ϕ. The order parameter remains zero up to a concentration of $\phi \approx 3.68$, where it jumps discontinuously to 0.6. As shown in Fig. 1(a), this is a first order transition from an isotropic phase, with $S = 0$ for $\phi < 3.68$, to a nematic phase $S \neq 0$ for $\phi > 3.68$.[27] Minimizing F and using asymptotic expansions,

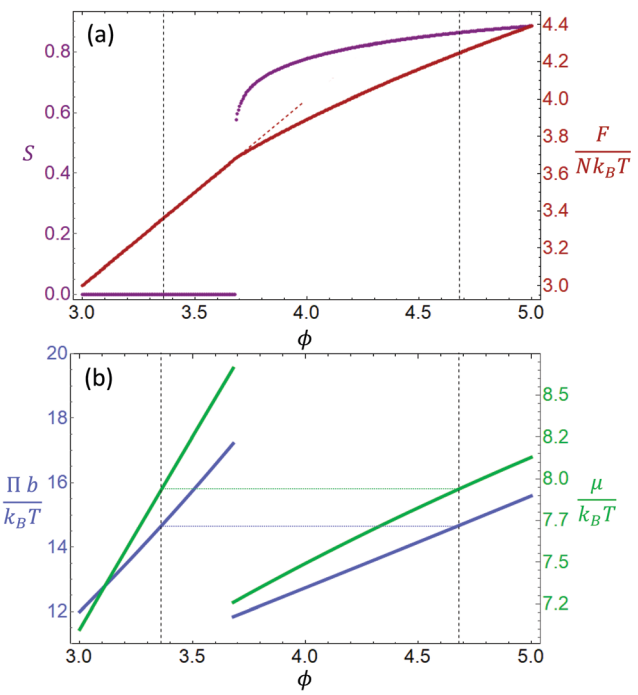

Fig. 1 (a) Scaled free energy of the Onsager theory as a function of the scaled concentration ϕ for the equilibrium state (solid red) and isotropic phase (dashed red). Order parameter S in purple. (b) Osmotic pressure (blue) and chemical potential (green) for isotropic and nematic phases at given concentration ϕ. The coexistence boundaries are highlighted with a dashed line.

eqn (2) and (3) become

$$\Pi = \frac{k_B T}{b}\begin{cases} \phi + \phi^2 & \phi < 3.68 \\ 3\phi + \dfrac{15\pi}{16\phi} & \phi > 3.68 \end{cases}, \quad (4)$$

and

$$\mu = k_B T\begin{cases} \log\phi + 2\phi & \phi < 3.68 \\ \log\dfrac{4}{\pi} + 3 + 3\log\phi + \dfrac{15\pi}{32\phi^2} & \phi > 3.68 \end{cases}. \quad (5)$$

Fig. 1(b) shows how Π and μ change as a function of the concentration ϕ.

Simultaneously equating the pressure and chemical potential of the two phases gives the value of phase coexistence ϕ_I = 3.36 and ϕ_N = 4.68. These boundary concentrations are slightly different from the values of 3.34 and 4.48 obtained by Onsager,[10] since they are derived from a first order expansion of the quantities described above. This approximation allows writing Π and μ as functions of ϕ. A more detailed discussion is included in the ESI.† In a system where $\phi < \phi_I$, the order parameter is S = 0, and therefore it is in an isotropic state. Conversely, for $\phi > \phi_N$ the system is in a completely nematic state, with $S > 0.8$. For concentrations in between the two values, the system is said to be in a supersaturated state and it will undergo phase separation into two distinct phases, equilibrating at a concentration between the two boundary concentrations. The isotropic state becomes metastable for $3.68 < \phi < 4$,[28] as shown by the dotted red line in Fig. 1(a), therefore nucleation and growth will only occur if the supersaturated solution concentration is in between these values, and for concentration beyond $\phi > 4$ the system will phase separate following spinodal decomposition.[29]

3 Nucleation

The process of phase separation under the present analysis, in the context of LLCPS, starts with the nucleation of tactoids; more generally, both nucleation and growth and spinodal decomposition are possible. The mechanism of formation of colloidal droplets has been extensively studied thermodynamically.[30] In the context of anisotropic, homogeneous liquid crystalline droplets of volume V_p, the free energy F_W has been calculated by Wulff[31] and reported by Prinsen and van der Schoot[14] as

$$F_W = \gamma V_p^{2/3}\begin{cases} 2\left(\dfrac{36}{35}\pi\left(7\sqrt{\omega} + \dfrac{1}{\sqrt{\omega}}\right)\right)^{1/3} & \omega \geq 1 \\ 6^{2/3}\left(\dfrac{\pi}{35}(\omega^3 - 7\omega^2 + 35\omega + 35)\right)^{1/3} & 0 < \omega < 1. \end{cases} \quad (6)$$

where γ is the isotropic surface tension and ω is the adimensional anchoring strength.[19]

Let V_p be a fixed volume at concentration $\phi \geq 3.68$, initially in a supersaturated isotropic state. From eqn (1) the change in free energy ΔF_V, that occurs when the rods align into a nematic phase, can be expressed as

$$\Delta F_V = -V_p \frac{k_B T}{b} g(\phi), \quad (7)$$

where g is a number depending only on ϕ. It is the difference from the dashed and solid red line in Fig. 1(a). The total change in free energy becomes

$$\Delta F = \Delta F_V + F_W = -AV_p + BV_p^{2/3}. \quad (8)$$

where A and B are the other factors in eqn (6) and (7), which do not depend on V. Since ΔF_V is always negative, while F_W is always positive, there exists a minimum volume beyond which the tactoid will become stable.[32] This volume V_{min} corresponds to the value that nullifies the derivative, *i.e.* $\frac{d\Delta F}{dV_p} = 0$. With the previous symbolism it can be written as $V_{min} = \left(\frac{2B}{3A}\right)^3$. For volumes lower than V_{min}, the free energy increases with an increase in the size, thus the droplet shrinks redissolving in the solution, while for volumes larger than V_{min}, Δ_F decreases, leading to a growth behavior. A more detailed discussion on nucleation of hard rod systems can be found in ref. 33 The surface tension γ can be linked to the geometry of the rods as $\gamma \sim \frac{k_B T}{LD}$, from Van der Shoot's previous work.[34] The minimum volume for nucleation scales as

$$V_{min} \sim L^3. \quad (9)$$

For BLG,[20] where L = 550 nm and ω = 1.3, we can compute the above mentioned quantities and obtain a minimal volume of V_{min} = 19.6 μm^3, for a nucleating concentration of ϕ = 3.8. For C-CNC,[21] where L = 450 nm and ω = 0.8, the minimal volume is V_{min} = 8.9 μm^3, while for S-CNC,[21] where L = 330 nm with ω = 0.5, we obtain V_{min} = 3.0 μm^3. The resulting shape of the curve is represented in Fig. 2(a). This quantity corresponds to the minimal volume needed by a homogeneous nematic tactoid to form a surface and initiate phase separation without redissolving into the isotropic solution. From the available experimental data, as shown in Fig. S3 (ESI†), the smallest volume measured for BLG tactoids was 80 μm^3, while it was 20 μm^3 for C-CNC, in line with the theoretical predictions. In the case of S-CNC, we cannot make a reasonable comparison, since the smallest tactoids are extremely elusive to experimental characterization, due to the faster equilibration of this system.[35]

4 Growth phase

The nematic tactoids, nucleated from the supersaturated solution, undergo a growth process which increases their size and concentration, until an equilibrium between the chemical potential and pressure is reached, and therefore the boundaries of phase coexistence predicted using the Onsager theory. The growth phenomenon has been studied extensively and many models have been formulated to describe the increase in size in crystalline domains;[32,36] a review of single-phase

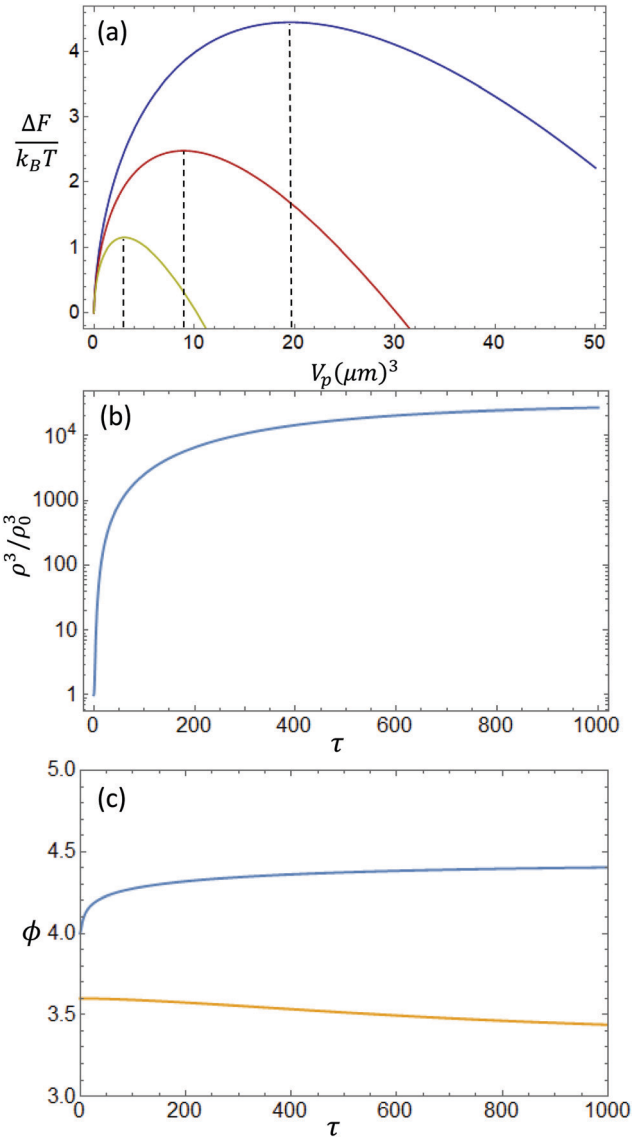

Fig. 2 (a) Difference in the free energy for a nucleated nematic domain from the isotropic background as a function of the volume V_p, for the BLG system (blue), C-CNC (red) and S-CNC (yellow). (b) Time evolution of the scaled volume ρ^3 over the initial condition $\rho(0)^3$; (c) Time evolution of the concentration ϕ for the nematic phase (blue) and the isotropic phase (orange). For both graphs, have been used the scaled variables ρ (eqn (12)) and τ as defined in the Appendix.

growth theories has been presented by Atkinson.[37] To model the kinetics of this binary system, composed of a solvent and a solute, we resort to the thermodynamic extremum principle[38] to derive the dynamics of change in volume and concentration of the droplets. This approach is based on the work of Onsager[39] and has been implemented to describe growth in multi-component multi-phase systems,[40] albeit not in liquid–liquid or in liquid–liquid crystalline phase separation. The full derivation is reported in the Appendix, and here, we summarize the most important steps.

In this section, we will assume that the tactoids are spherical in shape, thus only with isotropic surface tension $\frac{dE}{dV_p} = \frac{2\gamma}{R}$. The real shape of the droplets may be taken into account by adjusting the coefficients when the surface is involved. However, this correction will depend on the volume and the particular system under study,[21] therefore overly complicating the analysis. The growth is influenced by three quantities: the difference in osmotic pressure $\Delta\Pi$, the chemical potential $\Delta\mu$ between the nematic and isotropic phase, and the external pressure, in this case, it is the Laplace pressure generated by the isotropic surface tension.[41]

We consider a model system of a single nematic droplet n, of a size V larger than the critical nucleus size, growing in a continuous supersaturated isotropic phase i. The free energy can be written as the sum of three components: the free energy of the two phases and the free energy of the interaction F_γ, given by the surface energy $F_\gamma = 4\pi R^2\gamma$. The total free energy F_T of this system can be written as

$$F_T = F_i + F_n + F_\gamma. \tag{10}$$

The total volume and number of solute molecules are fixed, therefore F_T becomes

$$F_T = \frac{4\pi}{3}R^3\left(\frac{\phi}{b}\Delta\mu - \Delta\Pi\right) + 4\pi R^2\gamma, \tag{11}$$

where the terms not depending on R and ϕ have been omitted. We define R^* as

$$R^* = \frac{2b\gamma}{k_B T}, \tag{12}$$

which scales as a length $R^* \sim L$ with the previously used scaling argument. With a change of variables $R = R^*\rho$, we can write

$$F_T = \frac{4\pi}{3}R^{*3}\frac{k_B T}{b}\left(\rho^3(\phi\Delta\mu' - \Delta\Pi') + \frac{3}{2}\rho^2\right) \tag{13}$$

where $\mu = k_B T\mu'$ and $\Pi = \frac{k_B T}{b}\Pi'$. In this representation, for $\rho \ll 1$ the surface tension is the dominant term, while for larger sizes $\rho \gg 1$, the change in potentials becomes leading. The length R^* represents the characteristic length of the system and as shown in the previous section, the results of both classical nucleation theory and the following approach are based on this same length scale, since $R^* \sim L \sim V_{min}^{1/3}$.

The total free energy, in this formulation, depends only on ρ and ϕ. We can obtain the evolution equations of these two quantities using the modelling proposed by Svoboda *et al.*[40] where the dynamical system can be written from the derivatives of a dissipation function Q depending on the flow of the solute and solvent.

In Fig. 2(b and c) are plotted the curves of $(\rho/\rho(0))^3(t)$ and $\phi(t)$ representing the numerical solutions of the presented differential equations. The initial conditions chosen are $\rho(0) = 10$, $\phi(0) = 4$ and $\phi_i(0) = 3.6$. Panel A represents the time evolution of the scaled volume ρ^3 from the initial condition of $\rho^3(0)$, and the volumes increase by 4 orders of magnitudes before reaching a horizontal asymptote. The choice of initial conditions depends on the free energy of eqn (13). For small volumes, *i.e.* smaller than the critical nucleus size, the surface tension will be strong enough, leading to a dissolution of the droplet.[36,42] In Fig. 2(c) are plotted the

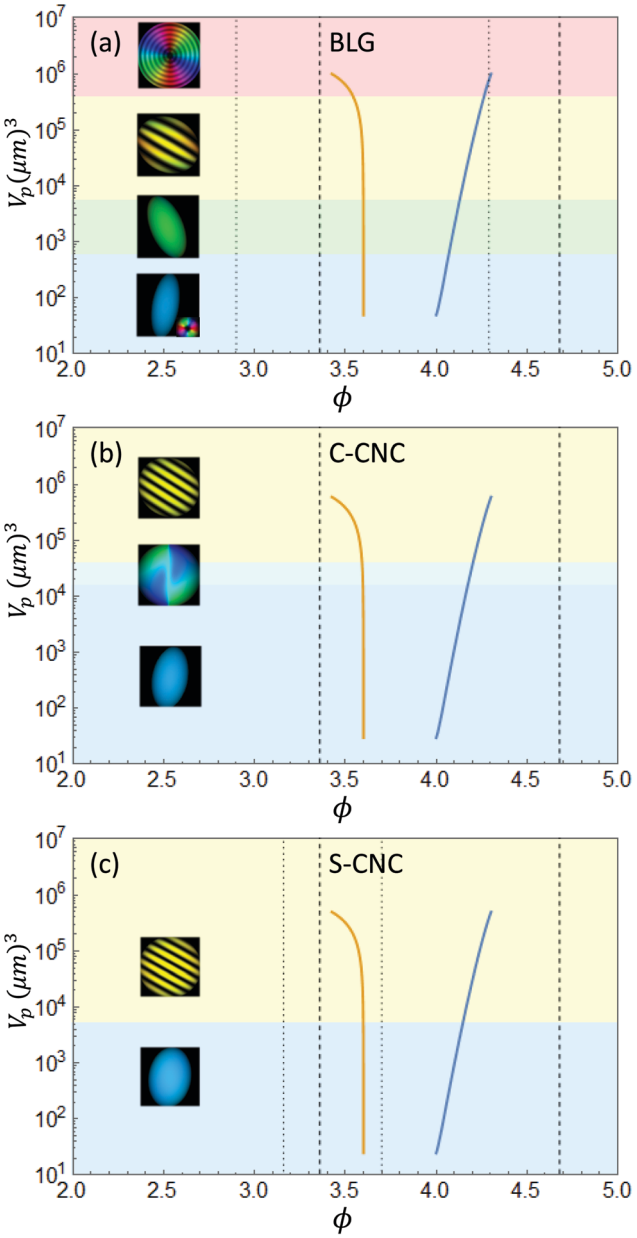

Fig. 3 Change in concentration ϕ with the volume V_p for the analyzed systems: BLG (a), C-CNC (b) and S-CNC (c). The blue line represents the nematic phase, while the orange the isotropic phase. Additionally, the morphology of the droplet at the given volume is represented with a simulated PolScope image and a colored background, as in Fig. 1. The dashed lines represent the boundaries of the coexistence phase, as described by the theory ϕ_I = 3.36 and ϕ_N = 4.68. The dotted line represents the experimental boundaries measured by Bagnani *et al.*[21]

concentrations of the nematic droplet (in blue) and isotropic background (in orange). The concentration follows the same pattern as that of the volume, where it reaches an asymptote around 4.3. This is slightly lower than the boundaries presented in the previous paragraph, since the Laplace pressure caused by the surface tension has to be balanced by an additional difference in the osmotic pressure.[43]

From the estimates obtained from the nucleation theory, we can calculate the physical volume V_p, by setting $\frac{4\pi}{3}R^{*3}\rho^3 = V_p$, and thus obtain the change in concentration with the volume of the droplet V_p. The results are shown in Fig. 3, where the concentrations of nematic and isotropic phases are plotted with the volume of the nematic phase. These two lines represent the binodal curve of the system undergoing the growth process, where with an increase in the volumes the concentration in the nematic phase increases, while the concentration in the isotropic phase slowing decreases. The real dynamics of phase separation depends on many different quantities: the diffusion coefficients, the total volume of solution and the initial conditions, which are different in every system. Also, in a real system, a population of tactoids with different volumes would nucleate and grow, possibly colliding and forming new tactoids. In this analysis, we considered the growth of a single droplet of a given concentration and volume immersed in a supersaturated isotropic solution, therefore the effects of having a population of droplets interacting have not been considered and it is outside the scope of this analysis.

5 Discussion

LLCPS behaviour has been observed in multiple biological colloids, such as viruses,[44] DNA,[45] cellulose nanocrystals (CNC)[21,46] and amyloid fibrils.[18,26] Understanding the underlining mechanisms in the formation of nematic and cholesteric tactoids is extremely important for functionalizing these materials, especially protein-based biocolloids, which have become increasingly significant in food,[47] medicine[48] and biological industries.[49]

In what follows, we show the prediction on the total free energy of the system during evolution of the volume of the three colloids considered, which is now obtained based on the theoretical approach described in the earlier sections, by taking into account liquid crystalline interactions within the growing droplets. The evaluation of the free energy follows the same approach used in the work of Bagnani *et al.*,[20,21] where an extensive analysis has been performed to understand the change in shape and in the configuration of the nematic director field and how these different phases appear.

The free energy functional used is the Frank–Oseen bulk energy, composed of three independent terms proportional to the elastic constants K_1, K_2 and K_3,[19] coupled with an anisotropic surface energy.[50]

$$F_{FO} = \int_V K_1(\nabla\cdot\vec{n})^2 + K_2(\vec{n}\cdot\nabla\times\vec{n} - q_\infty)^2 + K_3(\vec{n}\times\nabla\times\vec{n})^2 \mathrm{d}V + \gamma\int_{\partial V} 1 + \omega(\vec{n}\cdot\vec{\nu})^2 \mathrm{d}S \quad (14)$$

where $\vec{n}$ is the nematic director field and q_∞ is the pitch wave number. Additional details can be found in the ESI† of ref. 20 This functional correctly predicts the shape and nematic field configuration for all the classes of nematic and cholesteric tactoids

Table 1 Elastic constants and surface tension parameters for BLG, C-CNC and S-CNC, used in eqn (14), obtained from ref. 21

	BLG	C-CNC	S-CNC
K_1 (pN)	2.0	0.6	2.6
K_2 (pN)	2.7	0.1	0.02
K_3 (pN)	1.5	1.0	2.3
γ (μN m^{-1})	0.34	0.24	0.13
ω	1.3	0.8	0.5

found experimentally.[20] The values of the constants used can be found in ref. 21, for the three systems under study and are reported in Table 1.

The total free energy F_{FO} at each volume has been plotted for each system in Fig. 4 (black line). However, it can be noted that elastic distortions and the anisotropy of the surface account for about one tenth of the total energy, even for homogeneous tactoids as shown in Fig. S2 (ESI†). Therefore, the approximation used in the previous paragraph, that is including only the surface energy of the tactoid, is appropriate for our case. To better visualize the transitions, the total free energy F_{FO} has been reduced by the isotropic surface free energy of a sphere of equivalent volume and is plotted with a grey line. This line represents the energy contributions of elastic distortions and anisotropic surface tension. The various classes of tactoids are highlighted with a PolScope simulation,[20] while their aspect ratios are included in Fig. S3 (ESI†).

BLG amyloid fibrils form nematic tactoids with a rich palette of morphologies, including a variety of cholesteric phase configurations.[20] These four different classes of tactoids are called homogeneous, bipolar, uniaxial and radial cholesteric. These four classes of tactoids, see Fig. S3(a) (ESI†), appear at increasing volumes with decreasing aspect ratios. It is interesting to note the two kinks in the grey line, corresponding to the phase transitions into uniaxial cholesteric and radial cholesteric morphologies. According to the Ehrenfest classification of phase transitions,[51] the morphology transitions from bipolar to uniaxial cholesteric and from uniaxial to radial cholesteric are first order phase transitions, with a discontinuous jump in the first derivative of the free energy, which is reflected in a discontinuous jump in the observed aspect ratios, see Fig. S3(a) (ESI†). In the span of volumes where homogeneous turn into bipolar the derivative changes smoothly, implying that the phase transition is of an higher order, as already intuited by Prinsen and van der Schoot.[14]

A similar rich palette of structure has been observed in cholesteric phases formed by carboxylated and sulfurated cellulose nanoscrystals.[21] The tactoid morphologies of C-CNCs are named homogeneous, radial nematic and uniaxial cholesteric,[21] see Fig. S3(b) (ESI†). A similar energy landscape is shown in Fig. 4(b). Here, we observe a discontinuous derivative in the transition into radial nematic and another transition into the uniaxial cholesteric. Lastly, in the S-CNCs only two configurations appear, homogeneous and uniaxial cholesteric, see Fig. S3(c) (ESI†), where a first order transition is observed from one morphology to the other, as shown in Fig. 4(c).

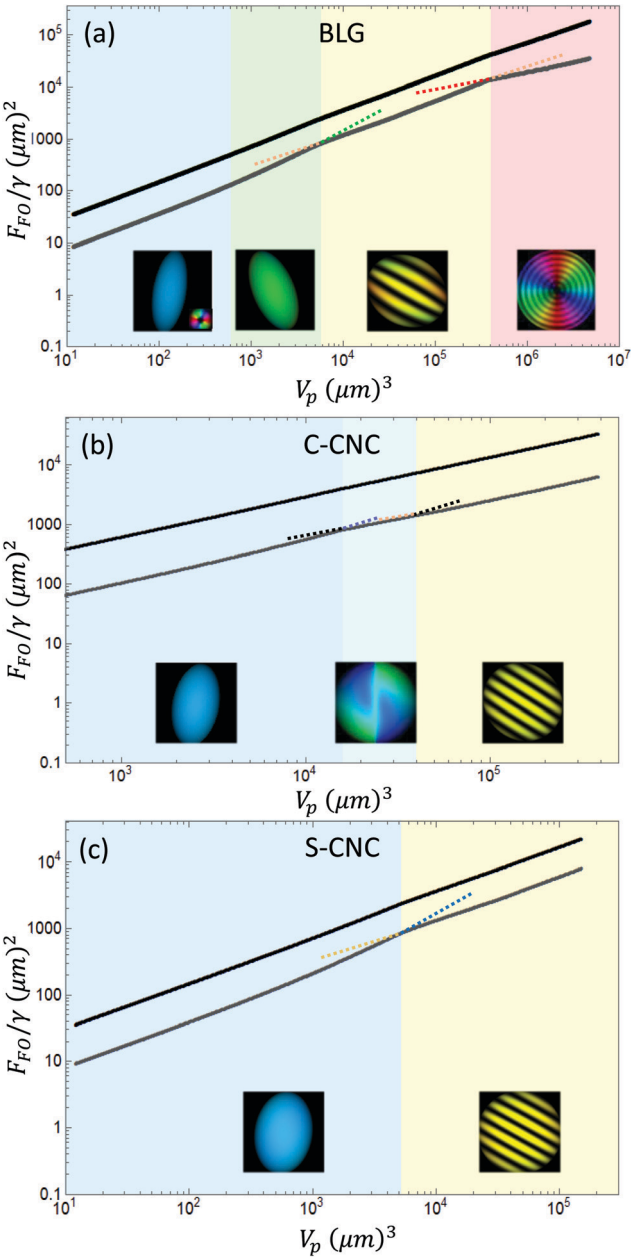

Fig. 4 The total free energy F_{FO}/γ for different volumes (V_p) is marked in black and the sum of elastic distortions and anisotropic surface energy is marked in grey, for BLG (a), carboxylated (b) and sulfurated (c) CNC. The colored background represents the range of volumes over which a particular morphology of the tactoid is observed,[21] integrated with a PolScope simulation of the particular configuration.[20]

Experimentally, liquid crystalline droplets have been observed under a cross-polarized microscope and for cholesteric configurations, the pitch has been measured from the generated images, as twice as the distance from band to band, and are plotted in Fig. 5 with their respective volumes. The additional details and methods regarding the experimental systems are given in ref. 21.

The tactoids obtained from BLG amyloid fibrils and carboxylated CNCs show a decreasing behavior of the pitch for

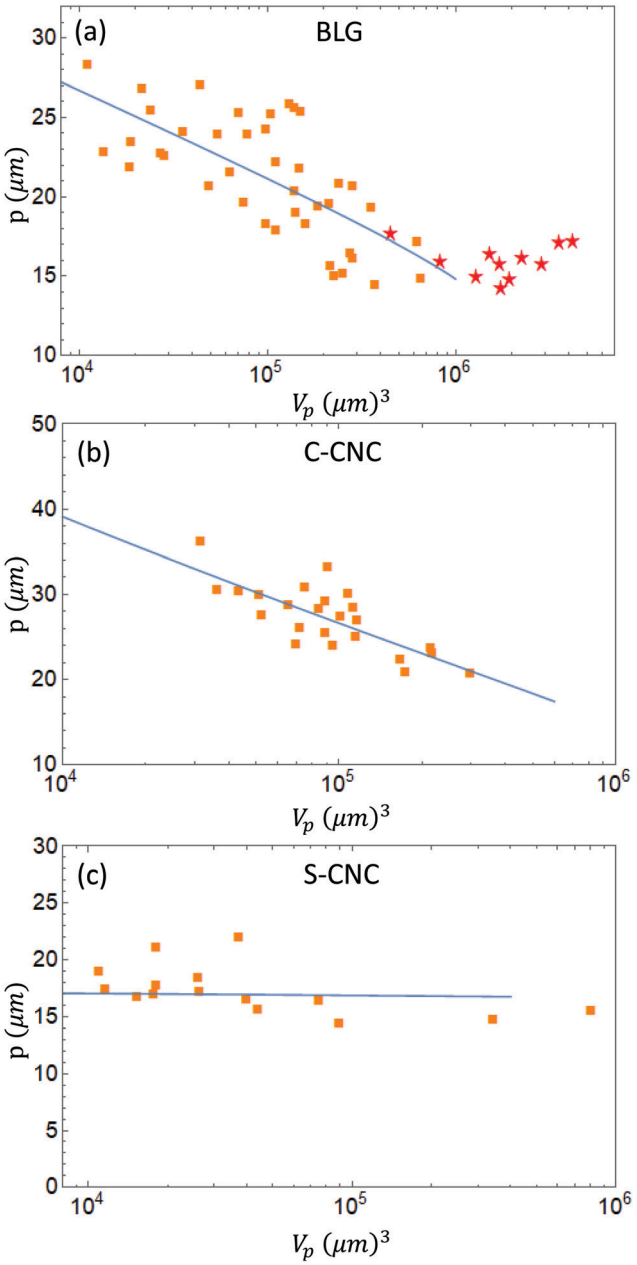

Fig. 5 Periodicity of the cholesteric tactoids p as a function of the volume V_p for BLG (a), C-CNC (b), and S-CNC (c) with the fitted lines obtained by the theory. The fitting parameters are reported in the ESI.† The orange boxes (■) symbolize the uniaxial cholesteric droplets, while the red stars (★) symbolize the radial cholesteric droplets.[21]

increasing volumes. The BLG system reaches eventually the radial cholesteric configuration where the pitch does not decrease further. In contrast, the sulfurated cellulose shows a constant pitch, over two orders of magnitude in volumes. Previous attempts to connect this feature of cholesteric droplets with the constraint imposed by the confined geometry failed.[18,20] Based on the theoretical framework introduced here, we now show that it becomes possible to link the change in pitch observed with the change in concentration during growth. From the work of Nystrom *et al.*[52] we assume a pitch dependence of the concentration of the form $p \sim \phi^{-1}$, even though there is much debate around the correct exponent.[44,53,54] As a general formula, we adopt

$$p(V) = \frac{K}{\phi(V_p) - v} + q \tag{15}$$

The expression for $\phi(V_p)$ is obtained from the blue line of Fig. 5. The results are plotted in Fig. 3 with the experimental data of the pitch of cholesteric tactoids of the systems analyzed. The quantities K, q, v are the fitted variables, which are included in Table S1 of the ESI.† For the case of BLG, the modeled growth stops at a volume of 10^6 μm^3, with a pitch of p = 15 μm. In the fit obtained, the blue line is stopped at that maximum value, reached by the size of the droplet when the process halts. In this frame, the radial cholesteric morphology represents the last stage of growth, where the equilibrium concentrations are reached, therefore from this volume there are no further changes in the pitch. A similar behavior is observed in C-CNCs, although no radial configuration has been observed. Lastly, the S-CNC system results in a straight horizontal line from the theory. In this system the pitch remains constant for two possible reasons: as reported in ref. 21, the experimental coexistence boundaries are 3.16 and 3.70, for the isotropic and nematic phases, much closer than the predicted values from the Onsager theory and hence, much closer to the final asymptotic equilibrium conditions. This fact implies a possible change in the concentration in the nematic phase of maximum 20%, which would generate a shrinking of the pitch of the same magnitude, well within the standard deviation of the experimental data. The difference between the theoretical boundaries, obtained using the Onsager theory, and the experimentally measured ones can explain the different growth regimes between different systems. BLG, as shown in Fig. S3(a) (ESI†), grows in volume over six orders of magnitude, while the growth in cellulose systems is much more constrained. In fact, the evolution of sulfurated cellulose is more rapid than that of β-lactoglobulin, resulting in a faster equilibration of the cholesteric configurations.[35]

6 Conclusions

We formulated a general model to describe the nucleation, growth, order–order transitions and change in concentration of nematic tactoids immersed in an isotropic phase in the coexistence regime by taking into account how the chemical potential, osmotic pressure and surface tension influence the diffusion of the solvent and solute inside the droplets. With the application of thermodynamic extremum principle[38] and the Onsager theory of liquid crystals,[10] we formulated the kinetic equations for the growth of tactoids. The growth behaviour is linked to an increase in the concentration in the nematic phase, accompanied by a consequent decrease in the concentration of the isotropic phase. The resulting effect is the change in periodicity of the cholesteric droplets with increasing volumes. This model was applied and validated by three

different systems of biocolloidal liquid crystals, namely β-lactoglobulin amyloid fibrils and carboxylated and sulfurated cellulose nanocrystals. The first two systems displayed a decreasing behavior of the pitch with an increasing droplet size[18,46] which until this work has remained unexplained. With the elucidation of how the tactoidal droplets grow, we then applied the previous results obtained by the variational theory of the Frank–Oseen to benchmark the experimentally observed order–order transitions and to elucidate the thermodynamic nature of these transitions. This work introduces for the first time a non-equilibrium status of the tactoids, providing new insight into the dynamics of phase separation and cholesteric pitch evolution, useful for understanding and expanding the capabilities of using cholesteric liquid crystals as a template for nanotechnology and for the synthesis of new, functional biomaterials.

Conflicts of interest

There is no conflict of interest to declare.

Appendix

Following the work of Svoboda *et al.*,[40] we set the starting point for the equations for the growth by writing the total free energy of the system. We consider a biphasic system composed of a nematic phase n confined in a sphere of radius R of concentration $c = N/V = \phi/b$ and a isotropic phase i of volume V_i. The two phases are separated by a surface, whose energy is $F_\gamma = 4\pi R^2\gamma$.

$$F_T = F_i + F_n + F_\gamma \tag{16}$$

Additionally, the free energy F of the two phases can be rewritten as the sum of two terms $F = N\mu - V_p\Pi$ (see the main text).

$$F_T = N_i\mu_i - V_i\Pi_i + \frac{4\pi R^3}{3}(c\mu_n - \Pi_n) + 4\pi R^2\gamma \tag{17}$$

Since the total volume V_T and total number of solute molecules N_T are fixed, the isotropic quantities can be rewritten as

$$N_i = N_T - \frac{4\pi R^3}{3}c \quad \text{and} \quad V_i = V_T - \frac{4\pi R^3}{3}. \tag{18}$$

By regrouping the important quantities, we get

$$F_T = N_T\mu_i - V_T\Pi_i + \frac{4\pi}{3}R^3(c\Delta\mu - \Delta\Pi) + 4\pi R^2\gamma. \tag{19}$$

The Δ implies the difference of the potentials between the nematic phase and the isotropic phase.

The total free energy depends only on R and c. We can obtain the evolution equations of these two quantities using the modelling proposed by Svoboda *et al.*,[38] based on the Onsager extremum principle,[39] where the time evolution of the system comes from a set of linear equations

$$\frac{\partial F_T}{\partial R} = -\frac{1}{2}\frac{\partial Q}{\partial \dot{R}} \quad \frac{\partial F_T}{\partial c} = -\frac{1}{2}\frac{\partial Q}{\partial \dot{c}} \tag{20}$$

where the dot represents the time derivative and Q the dissipation function.

From Svoboda *et al.* work,[38] the dissipation function for diffusive flows can be written as

$$Q = k_B T\sum_l \int_{V_T} \frac{j_l^2}{c_{ll}}V. \tag{21}$$

where l is the diffusion coefficient and j_l is the flow of the component indexed with l. In our case it can be the solvent w or solute s. We can split the integral as the sum of an integral in the nematic phase and one in the isotropic phase:

$$Q = Q_i + Q_n. \tag{22}$$

Since the total amount of volume is occupied by the solvent or solute, we can write

$$V_p = \nu_s N_s + \nu_w N_w \tag{23}$$

with $\nu_{s,w}$ being the volume occupied by a single molecule. This constraint leads to two relationships between c_s and c_w

$$c_w = \frac{1 - \nu_s c_s}{\nu_w} \quad \text{and} \quad \dot{c}_w = -\frac{\nu_s}{\nu_w}\dot{c}_s \tag{24}$$

In the nematic phase, the volume is a sphere and the flow can be simply rewritten as $j_l = \frac{r}{3}\dot{c}_l$. By rewriting eqn (21) in the nematic phase, we get

$$Q_n = \frac{4\pi k_B T R^5}{45}\frac{\dot{c}_s^2}{\mathbb{D}_n}; \tag{25}$$

with $\mathbb{D}_n^{-1} = \left(\frac{1}{c_{ss}} + \left(\frac{\nu_s}{\nu_w}\right)^2\frac{1}{c_{ww}}\right)$.

In the nematic phase, the total number of molecules of the compound l is $N_l = \frac{4\pi R^3}{3}c_l$, thus the rate of change of N_l is

$$\dot{N}_l = 4\pi R^2\left(\dot{R}c_l + \frac{R}{3}\dot{c}_l\right). \tag{26}$$

This rate of change of number comes from the increase in volume and a diffusive flow through the surface[40]

$$\dot{N}_l = 4\pi R^2\left(\dot{R}c_{l,i} + j_l^*\right), \tag{27}$$

where $c_{l,i}$ is the concentration of l in the isotropic phase i. The flow at the surface can be written as

$$j_l^* = \dot{R}(c_l - c_{l,i}) + \frac{R}{3}\dot{c}_l \tag{28}$$

The flow at a distance r from the center of the sphere where $r > R$ is $j_l = \frac{R^2}{r^2}j_l^*$. This last expression can be used in eqn (21) to

obtain the dissipation function in the isotropic phase Q_i:

$$Q_i = 4\pi k_B T R^3 \times \left(\frac{\left(\dot{R}(c_s - c_{s,i}) + R\frac{\dot{c}_s}{3}\right)^2}{c_{s,is,i}} + \frac{\left(\dot{R}(c_w - c_{w,i}) + R\frac{\dot{c}_w}{3}\right)^2}{c_{w,iw,i}} \right), \quad (29)$$

using $\mathbb{D}_i^{-1} = \frac{1}{c_{s,is,i}} + \left(\frac{\nu_s}{\nu_w}\right)^2 \frac{1}{c_{w,iw,i}}$ and eqn (24), we obtain

$$Q_i = \frac{4\pi k_B T R^3}{\mathbb{D}_i}\left((c - c_i)^2 \dot{R}^2 + \frac{R^2}{9}\dot{c}^2 + \frac{2}{3} R\dot{R}\dot{c}(c - c_i) \right) \quad (30)$$

The derivatives of $Q = Q_i + Q_n$ are

$$\frac{1}{2}\frac{\partial Q}{\partial \dot{R}} = \frac{4\pi k_B T R^3}{\mathbb{D}_i}\left(\frac{R}{3}(c - c_i)\dot{c} + (c - c_i)^2 \dot{R} \right) \quad (31)$$

$$\frac{1}{2}\frac{\partial Q}{\partial \dot{c}} = \frac{4\pi k_B T R^3}{\mathbb{D}_i}\left(\frac{R}{3}(c - c_i)\dot{R} + \frac{R^2}{9}\dot{c} \right) + \frac{4\pi k_B T R^5}{45\mathbb{D}_n}\dot{c} \quad (32)$$

The derivatives of the free energy of eqn (19) are

$$\frac{\partial F_T}{\partial R} = 4\pi R^2 \left(\frac{2\gamma}{R} + c\Delta\mu - \Delta\Pi \right) \quad (33)$$

$$\frac{\partial F_T}{\partial c} = \frac{4\pi}{3} R^3 \Delta\mu. \quad (34)$$

Using eqn (20) we get

$$\frac{k_B T R}{\mathbb{D}_i}\left(\frac{R}{3}(c - c_i)\dot{c} + (c - c_i)^2 \dot{R} \right) = \Delta\Pi - \frac{2\gamma}{R} - c\Delta\mu \quad (35)$$

$$\frac{k_B T R}{\mathbb{D}_i}\left((c - c_i)\dot{R} + \frac{R}{3}\dot{c} \right) + \frac{k_B T R^2}{15\mathbb{D}_n}\dot{c} = -\Delta\mu \quad (36)$$

From the previous equations, it is possible to write the rate of change of concentration and radius

$$\dot{R} = \frac{\mathbb{D}_n}{k_B T R (c - c_i)^2}\left(\frac{\mathbb{D}_i}{\mathbb{D}_n}\left(\Delta\Pi - \frac{2\gamma}{R} - c\Delta\mu \right) + 5\left(\Delta\Pi - \frac{2\gamma}{R} - c_i\Delta\mu \right) \right) \quad (37)$$

$$\dot{c} = \frac{15\mathbb{D}_n}{k_B T R^2 (c - c_i)}\left(\Delta\Pi - \frac{2\gamma}{R} - c\Delta\mu \right). \quad (38)$$

With a suitable change of variables, the equations can be rewritten in a more compact form

$$\dot{\rho} = \frac{1}{(\phi - \phi_i)^2 \rho}\left(\kappa\left(\Delta\Pi' - \frac{1}{\rho} - \phi\Delta\mu' \right) + 5\left(\Delta\Pi' - \frac{1}{\rho} - \phi_i\Delta\mu' \right) \right) \quad (39)$$

$$\dot{\phi} = \frac{15}{(\phi - \phi_i)\rho^2}\left(\Delta\Pi' - \frac{1}{\rho} - \phi\Delta\mu' \right); \quad (40)$$

where

$$\rho = R/R^* \quad \text{with } R^* = \frac{2\gamma b}{k_B T} \quad (41)$$

$$\tau = t/t^* \quad \text{with } t^* = \frac{\mathbb{D}_n (k_B T)^2}{4\gamma^3} \quad (42)$$

and $\kappa = \mathbb{D}_i/\mathbb{D}_n$, $\Delta\Pi = \frac{k_B T}{b}\Delta\Pi'$ and $\Delta\mu = k_B T \Delta\mu'$.

At each time, if the nematic phase has a volume $V_p = \frac{4\pi}{3}R^3$ and concentration ϕ, the isotropic phase has a concentration of

$$\phi_i = \frac{V_T \phi_0 - \phi V_p}{V_T - V_p} \quad (43)$$

where ϕ_0 is the initial concentration of the supersaturated solution and V_T is the total volume available.

Even though $\mathbb{D}_{i,n}$ depend on the concentration, we know from the Onsager theory that ϕ will range from 3.7 to 4.7 with a maximal increase of 27%. The isotropic phase ranges from 3.7 to 3.3 with a maximal decrease of 10%. From diffusion studies of hard rods we know that the diffusion coefficient remains constant at the coexistence and it is more than ten times larger compared to the nematic phase.[55] Therefore, we can assume that $\mathbb{D}_{i,n}$ will remain approximately constant during the process and the ratio κ will be much bigger than one.

For the results presented, we set $\kappa = 100$ and a scaled total volume of $V_T \Big/ \left(\frac{4}{3}\pi R^{*3}\right) = 10^8$.

Acknowledgements

The authors acknowledge support with Grant No. CRSII5_189917 from the Swiss National Science Foundation.

Notes and references

1 H. Tanaka, T. Araki, T. Koyama and Y. Nishikawa, *J. Phys.: Condens. Matter*, 2005, **17**, S3195.
2 A. R. Hemsley and P. C. Griffiths, *Philos. Trans. R. Soc., A*, 2000, **358**, 547–564.
3 C. Domb, *Phase transitions and critical phenomena*, Elsevier, 2000.
4 P. H. Poole, T. Grande, C. A. Angell and P. F. McMillan, *Science*, 1997, **275**, 322–323.
5 A. Mitus, A. Patashinskii and B. Shumilo, *Phys. Lett. A*, 1985, **113**, 41–44.
6 Y. Katayama, T. Mizutani, W. Utsumi, O. Shimomura, M. Yamakata and K.-I. Funakoshi, *Nature*, 2000, **403**, 170–173.
7 A. A. Hyman, C. A. Weber and F. Jülicher, *Annu. Rev. Cell Dev. Biol.*, 2014, **30**, 39–58.
8 H. Jing, Q. Bai, Y. Lin, H. Chang, D. Yin and D. Liang, *Langmuir*, 2020, **36**, 8017–8026.
9 S. Watanabe, H. Inami, K. Oiwa, Y. Murata, S. Sakai, O. Komine, A. Sobue, Y. Iguchi, M. Katsuno and K. Yamanaka, *Cell Death Dis.*, 2020, **11**, 1–15.

10 L. Onsager, *Ann. N. Y. Acad. Sci.*, 1949, **51**, 627–659.
11 T. Odijk, *Macromolecules*, 1986, **19**, 2313–2329.
12 P. W. Oakes, J. Viamontes and J. X. Tang, *Phys. Rev. E*, 2007, **75**, 061902.
13 V. Jamali, N. Behabtu, B. Senyuk, J. A. Lee, I. I. Smalyukh, P. van der Schoot and M. Pasquali, *Phys. Rev. E*, 2015, **91**, 042507.
14 P. Prinsen and P. van der Schoot, *Phys. Rev. E*, 2003, **68**, 021701.
15 A. Kaznacheev, M. Bogdanov and S. Taraskin, *J. Exp. Theor. Phys.*, 2002, **95**, 57–63.
16 L. Rossi, S. Sacanna and K. P. Velikov, *Soft Matter*, 2011, **7**, 64–67.
17 L. Tortora and O. D. Lavrentovich, *Proc. Natl. Acad. Sci. U. S. A.*, 2011, **108**, 5163–5168.
18 G. Nyström, M. Arcari and R. Mezzenga, *Nat. Nanotechnol.*, 2018, **13**, 330–336.
19 F. C. Frank, *Discuss. Faraday Soc.*, 1958, **25**, 19–28.
20 M. Bagnani, P. Azzari, S. Assenza and R. Mezzenga, *Sci. Rep.*, 2019, **9**, 1–9.
21 M. Bagnani, P. Azzari, C. De Michele, M. Arcari and R. Mezzenga, *Soft Matter*, 2021, **17**, 2158–2169.
22 P.-X. Wang, W. Y. Hamad and M. J. MacLachlan, *Nat. Commun.*, 2016, **7**, 1–8.
23 P. J. Flory and G. Ronca, *Mol. Cryst. Liq. Cryst.*, 1979, **54**, 289–309.
24 J. Straley, *Mol. Cryst. Liq. Cryst.*, 1973, **22**, 333–357.
25 A. N. Chester and S. Martellucci, *Phase transitions in liquid crystals*, Springer Science & Business Media, 2013, vol. 290.
26 M. Bagnani, G. Nystrom, C. De Michele and R. Mezzenga, *ACS Nano*, 2018, **13**, 591–600.
27 P. Palffy-Muhoray, E. G. Virga and X. Zheng, *J. Phys.: Condens. Matter*, 2017, **29**, 475102.
28 R. F. Kayser Jr and H. J. Raveché, *Phys. Rev. A: At., Mol., Opt. Phys.*, 1978, **17**, 2067.
29 M. P. Lettinga, K. Kang, A. Imhof, D. Derks and J. K. Dhont, *J. Phys.: Condens. Matter*, 2005, **17**, S3609.
30 J. W. Mullin, *Crystallization*, Elsevier, 2001.
31 G. Wulff, *Z. Krystallog.*, 1901, **34**, 449–530.
32 N. T. K. Thanh, N. Maclean and S. Mahiddine, *Chem. Rev.*, 2014, **114**, 7610–7630.
33 A. Cuetos, R. van Roij and M. Dijkstra, *Soft Matter*, 2008, **4**, 757–767.
34 P. van der Schoot, *J. Phys. Chem. B*, 1999, **103**, 8804–8808.
35 S. A. Khadem, M. Bagnani, R. Mezzenga and A. D. Rey, *Nat. Commun.*, 2020, **11**, 1–10.
36 I. M. Lifshitz and V. V. Slyozov, *J. Phys. Chem. Solids*, 1961, **19**, 35–50.
37 H. Atkinson, *Acta Metall.*, 1988, **36**, 469–491.
38 J. Svoboda and I. Turek, *Philos. Mag. B*, 1991, **64**, 749–759.
39 L. Onsager, *Phys. Rev.*, 1931, **37**, 405.
40 J. Svoboda, F. Fischer, P. Fratzl and E. Kozeschnik, *J. Mater. Sci. Eng. A*, 2004, **385**, 166–174.
41 A. Katchalsky and P. F. Curran, *Nonequilibrium thermodynamics in biophysics*, Harvard University Press, 2013.
42 A. Modlińska, A. M. Alsayed and T. Gibaud, *Sci. Rep.*, 2015, **5**, 1–10.
43 R. Mezzenga, B. M. Folmer and E. Hughes, *Langmuir*, 2004, **20**, 3574–3582.
44 Z. Dogic and S. Fraden, *Langmuir*, 2000, **16**, 7820–7824.
45 A. Goldar, H. Thomson and J. M. Seddon, *J. Phys.: Condens. Matter*, 2007, **20**, 035102.
46 G. Nyström, M. Arcari, J. Adamcik, I. Usov and R. Mezzenga, *ACS Nano*, 2018, **12**, 5141–5148.
47 Y. Cao and R. Mezzenga, *Adv. Colloid Interface Sci.*, 2019, **269**, 334–356.
48 G. G. Glenner, *N. Engl. J. Med.*, 1980, **302**, 1283–1292.
49 C. M. Dobson, *Nature*, 2003, **426**, 884–890.
50 E. G. Virga, *Variational theories for liquid crystals*, CRC Press, 1995, vol. 8.
51 P. Ehrenfest, *Proc. R. Acad. Sci. Amsterdam*, 1933, **36**, 153–157.
52 G. Nyström and R. Mezzenga, *Curr. Opin. Colloid Interface Sci.*, 2018, **38**, 30–44.
53 C. Honorato-Rios, J. Bruckner, C. Schütz, S. Wagner, Z. Tosheva, L. Bergström and J. P. Lagerwall, *Liquid Crystals with Nano and Microparticles*, World Scientific, 2017, pp. 871–897.
54 G. Chilaya, Z. Elashvili, L. Lisetski, T. Piliashvili and K. Vinokur, *Mol. Cryst. Liq. Cryst.*, 1981, **74**, 261–273.
55 M. P. B. van Bruggen, H. N. W. Lekkerkerker, G. Maret and J. K. G. Dhont, *Phys. Rev. E*, 1998, **58**, 7668–7677.

